Cancer Letters 442 (2019) 362–372

Contents lists available at ScienceDirect

Cancer Letters

journal homepage: www.elsevier.com/locate/canlet

Original Articles

Mitosis perturbation by MASTL depletion impairs the viability of thyroid tumor cells

Elena Cetti[a], Tiziana Di Marco[a], Giuseppe Mauro[a], Mara Mazzoni[a], Daniele Lecis[b], Emanuela Minna[a], Lucia Gioiosa[c], Silvia Brich[d], Sonia Pagliardini[a], Maria Grazia Borrello[a], Giancarlo Pruneri[d,e], Maria Chiara Anania[a,1], Angela Greco[a,*,1]

[a] Molecular Mechanisms Unit, Department of Research, Fondazione IRCCS Istituto Nazionale dei Tumori, Milan, Italy
[b] Molecular Immunology Unit, Department of Research, Fondazione IRCCS Istituto Nazionale dei Tumori, Milan, Italy
[c] Department of Applied Research and Technical Development, Fondazione IRCCS Istituto Nazionale dei Tumori, Milan, Italy
[d] Department of Pathology and Laboratory Medicine, Fondazione IRCCS Istituto Nazionale dei Tumori, Milan, Italy
[e] University of Milan, School of Medicine, Milan, Italy

ARTICLE INFO

Keywords:
MASTL
Mitotic catastrophe
Thyroid tumor cells
Non-oncogene addiction
Target validation

ABSTRACT

Even if thyroid tumors are generally curable, a fraction will develop resistance to therapy and progress towards undifferentiated forms, whose treatment remains a demanding challenge. To identify potential novel targets for treatment of thyroid cancer, in a previous study using siRNA-mediated functional screening, we identified several genes that are essential for the growth of thyroid tumor, but not normal cells. Among the top-ranking hits, we found microtubule associated serine/threonine kinase-like (MASTL), which is known to play an essential role in mitosis regulation, and is also involved in the DNA damage response. Herein, we examine the effects of MASTL depletion on growth and viability of thyroid tumor cells. MASTL depletion impaired cell proliferation and increased the percentage of cells presenting nuclear anomalies, which are indicative of mitotic catastrophe. Furthermore, MASTL depletion was associated with enhanced DNA damage. All these effects eventually led to cell death, characterized by the presence of apoptotic markers. Moreover, MASTL depletion sensitized thyroid tumor cells to cisplatin. Our results demonstrate that MASTL represents vulnerability for thyroid tumor cells, which could be explored as a therapeutic target for thyroid cancer.

1. Introduction

Inhibition of the cell cycle and, more specifically, of mitosis, has emerged as a promising strategy to hinder tumor cell growth and induce tumor cell death [1], as demonstrated by the use of microtubule-targeting agents as chemotherapy [2]. In addition to drugs that affect microtubule dynamics (e.g. taxanes, Vinca derivatives), several drugs that inhibit mitotic kinases, such as CDKs, Aurora and PLK kinases, have been explored clinically [1,3]. Among the plethora of kinases that play a role in mitosis regulation, microtubule associated serine/threonine kinase-like (MASTL) has recently received growing attention as a novel target for cancer therapy. MASTL is the mammalian orthologue of the *Greatwall* gene in *Drosophila* and *Xenopus* and is required for proper mitotic cell division: its inhibition induces delay in mitosis entry and leads to defects in chromosome segregation [4,5]. Indeed, MASTL has the crucial role of inhibiting the PP2A/B55 complex through activation of ENSA and ARPP19, thus allowing the phosphorylation of mitotic CDK-substrates and progression through mitosis [6]. Moreover, MASTL is also involved in the regulation of DNA damage response by promoting checkpoint recovery and progression into the cell cycle [7,8]. Besides ARPP19/ENSA phosphorylation and PP2A/B55 inhibition, Vera et al. have proposed an additional role of MASTL, which triggers AKT hyperactivation and cell transformation [9].

In comparison to other mitotic kinases, MASTL is less well characterized. However, in recent years, growing evidence of MASTL involvement in human cancer has been obtained. Overexpression of MASTL has been observed in solid tumors such as prostate, head and neck, colon, and breast cancer [9,10] and, in the latter, it has also been associated with patient poor prognosis [11]. Ectopic overexpression of MASTL was shown to promote the transformation of mammary glands cells [9]; more recently, MASTL has been proposed as a novel breast cancer oncogene whose activity, by driving chromosomal instability,

* Corresponding author. Fondazione IRCCS Istituto Nazionale dei Tumori, Via G.A. Amadeo, 42, 20133, Milan, Italy.
E-mail address: angela.greco@istitutotumori.mi.it (A. Greco).
[1] Co-last authors.

https://doi.org/10.1016/j.canlet.2018.11.010
Received 28 August 2018; Received in revised form 31 October 2018; Accepted 7 November 2018

invasion, and metastasis, results in more aggressive breast tumors and reduced patient survival [12].

Several authors have proposed MASTL as a novel target for cancer treatment. MASTL inhibition was shown to sensitize oral squamous cell cancer cells to cisplatin treatment [10], lung cancer cells to radiation therapy [13] and colon cancer cells to 5-fluorouracil [14]; in breast cancer cells, MASTL inhibition reduced cell growth both *in vitro* and *in vivo,* and enhanced radiosensitivity [11,15]. The increasing evidence of MASTL as a promising target for cancer therapy prompted a search for MASTL specific inhibitors. Based on the determination of the structure of the minimal MASTL kinase domain, Ocasio et al. [16] designed a small molecule inhibitor capable of inhibiting the kinase activity of MASTL. Very recently, an in silico approach identified several potential MASTL inhibitors of both natural and synthetic origin [17].

MASTL was recently identified by our group in a study using functional siRNA library screening to probe thyroid tumor cell vulnerability [18]. Thyroid cancer is the most frequent endocrine malignancy, characterized by an incidence that is constantly increasing worldwide [19]. The majority of thyroid tumors originate from epithelial follicular cells; the range of histological types includes, the well-differentiated papillary (PTC) and follicular (FTC) carcinomas, and the poorly differentiated (PDTC) and the anaplastic (ATC) carcinomas. The majority of thyroid tumors are represented by the differentiated histotypes, PTC and FTC, which generally have good prognosis as five-year survival rates in Europe and North America are over 98% [20]. Nevertheless, tumor recurrence can occur, as the tumor relapses in up to 20% of patients and distant metastases occur in about 10% of patients [21]. In contrast, patients with ATC have relatively poor prognosis, with median survival of 5 months and less than 20% are alive at 1 year after diagnosis [22]. Management of undifferentiated tumors is challenging for clinicians: although targeted therapies introduced in recent years have provided new opportunities for treatment, an effective therapy for aggressive lesions is still lacking [23].

To identify critical points for therapeutic intervention in thyroid cancer, we recently faced the non-oncogene addiction (NOA) paradigm, which asserts that, beyond oncogenes, the tumorigenic potential of cancer cells relies on genes that act in oncogenic pathways, but are not oncogenic themselves [24]. According to this concept, NOA genes are essential for the maintenance of the tumorigenic phenotype but not required for survival of normal cells; thus, they represent cancer vulnerabilities, which can be identified through functional RNA interference-based screening approaches [25,26]. Such genes can be explored as novel targets for therapeutic intervention. By screening a siRNA library on tumor and normal thyroid cell lines, we identified several genes which represent vulnerabilities for thyroid cancer [18,27]. MASTL was identified among the top-ranking hits. The MASTL gene is not mutated or overexpressed in thyroid tumors; its depletion impairs the growth of several thyroid tumor cell lines, irrespective of histotype or driving genetic lesion. Therefore, it represents an example of “non-oncogene addiction” in thyroid tumor cells.

To validate MASTL as a possible therapeutic target for thyroid carcinoma, we investigated the mechanisms by which MASTL depletion affects the viability of thyroid tumor cells.

2. Materials and methods

2.1. Sample collection and immunohistochemistry analysis

Thyroid tumor samples were collected at the Department of Pathology at Fondazione IRCCS Istituto Nazionale dei Tumori, Milan (INT). Neoplastic thyroid tissues were reviewed by an expert pathologist and classified according to the histopathological criteria of the World Health Organization [28]. Tumor collection (total n = 39) included: PTCs (n = 25); microPTCs (n = 2), ATCs (n = 4) and PDTCs (n = 8). For 28 of 39 samples, sections containing both tumor and normal thyroid tissue were available. All patients gave their written informed consent, and the study was approved by the independent ethic committee of INT. The immunohistochemical analysis was performed on formalin-fixed paraffin-embedded 2-μm tumor sections, subjected to antigen retrieval using 1 mM citrate buffer (pH 6), and then immunostained with a primary mouse monoclonal antibody anti-human MASTL (1:150; clone 4F9, MABT372, EMD Millipore Corporation, Temecula, CA, USA). Immunostaining was performed using a standard immunoperoxidase protocol followed by diaminobenzidine chromogen reaction (Dako REAL™ EnVision™ Detection System, K5007 Dako). The assessment of MASTL immunostaining (H-score), ranging from 0 to 300, was determined by a semiquantitative approach considering the percentage of positive tumor cells per slide (0%–100%), multiplied by the intensity pattern of staining (1, weak; 2, moderate; 3, intense) [29]. Images at 40X magnification were acquired with Aperio ScanScope® XT (Leica Biosystems, Germany).

2.2. Cell lines

The ATC-derived HTC/C3 and 8505C cell lines were cultured as previously described [18]. HTC/C3 cell line was purchased from Riken Cell Bank (Tsukuba, Japan); the 8505C cell line was obtained from Prof. A. Fusco (University Federico II, Naples, Italy). Cell lines were authenticated by short tandem repeat (STR) profiles using the Stem Elite ID System (Promega Corporation, Madison, USA) by the Fragment Analysis Facility of Fondazione IRCCS Istituto Nazionale dei Tumori. Cell lines matched their original profiles reported in the DSMZ Profile Database. Cell lines were periodically tested for mycoplasma contamination (PCR Mycoplasma Detection Set, TAKARA Bio Inc, Kusatsu, Japan) and found negative. Cell lines stably expressing H2B-GFP were generated by transfecting 2 μg of pEGFP-H2B plasmid (a gift from Dr. Geoff Wahl [30]) using Lipofectamine LTX (Invitrogen Life Technologies, Carlsbad, CA, USA), according to the manufacturer's instructions. Transfected cells were selected and cultured in medium containing G418 (500 μg/ml, Invitrogen Life Technologies, Carlsbad, CA, USA).

2.3. siRNA reagents and transfection

siRNA transfection was performed using 20 nM of siRNA oligos and Lipofectamine RNAiMAX reagent (Invitrogen Life Technologies, Carlsbad, CA, USA), according to the manufacturer's instructions. The siRNAs used were: siNT (D-0018-10-05), siMASTL#1 (J-004020-12, sequence 5′-CCAUUGAGACGAAAGGUUU-3′) and siMASTL#4 (J-004020-09, sequence 5′-CCAUUGAGACGAAAGGUUU-3′); siMASTL#5 (custom, sequence 5′-UGUGGAUUCUGGUGGGAUAdTdT 3′) from Thermofisher/Dharmacon Inc, Chicago, IL, USA.

2.4. Cell viability assay

Cells (1.9×10^5) were seeded in 60 mm dishes and transfected with siRNAs the following day. After 24 h, cells were harvested and plated in 96-well plates (2×10^3 cells/well). Growth rates were evaluated at different time points by CellTiter-Glo® Luminescent Cell Viability Assay (Promega Corporation, Madison, USA), as recommended by the supplier. Luminescence signals were acquired using a microplate reader (TecanUltra, Tecan Trading AG, Switzerland).

2.5. Crystal violet assay

Cells (1.2×10^4) were plated in 24-well plates and transfected with siRNAs the following day. Seven days later, cells were fixed with 3.7% formaldehyde solution (v/v) at room temperature for 15 min, washed with PBS, stained for 20 min with 0.1% crystal violet (w/v), and allowed to dry after washing with ddH_2O. Crystal violet was then dissolved in 10% acetic acid (v/v) for 30 min on a rocker, and then diluted 1:4 in ddH_2O. Optical density at $\lambda = 590$ nm was measured by using Ultrospec 2100 Pro spectrophotometer (GE Healthcare Bio-Sciences,

Pittsburgh, PA, USA).

2.6. Drug sensitivity assay

Cells (5×10^3 cells/well) were reverse transfected in 96-well plate with 20 nM siMASTL #5 oligo using Lipofectamine RNAiMAX reagent. After 48 h, cells were treated with cisplatin (Accord Healthcare, Italy) at concentrations ranging from 0 to 50 μM for 8505C cells, and from 0 to 10 μM for HTC/C3 cells, for an additional 48 h. For each cell line, drug cytotoxicity has been previously defined. Cells were then assessed for viability by CellTiter-Glo® Luminescent Cell Viability Assay (Promega Corporation, Madison, USA), as described above.

2.7. Immunofluorescence analysis

Cells growing on glass coverslips were transfected with siRNAs and fixed 120 (for HTC/C3) and 76 (for 8505C) hours later for 10 min with 4% paraformaldehyde (w/v). After permeabilization for 10 min with 1% BSA and 0.1% Triton X-100 in PBS, and incubation for 30 min with 1X blocking solution (2% BSA in PBS), cells were incubated for 1 h with the following primary antibodies: anti-β-tubulin (clone TUB 2.1: T4026, 1:400, Sigma Aldrich, St. Louis, MO, USA)-, anti-phosphorylated histone H3 (Ser10) (E173: ab32107, 1:1000, Abcam, Cambridge, UK), anti-γH2AX (clone JBW301, 1:400, Upstate, Merck-Millipore, Darmstadt, Germany). After washing with PBS, cells were incubated with Alexa Fluor® 546 rabbit (1:500, Invitrogen/Molecular Probes®) or Alexa Fluor® 488 mouse (1:500, Invitrogen/Molecular Probes®) secondary antibodies for 1 h. Slides were then prepared using ProLong Diamond Antifade mountant with DAPI (P36966, Molecular Probes®) and imaged with fluorescence microscopy (Eclipse E1000; Nikon Instruments, Inc. NY, USA). For evaluation of abnormal nuclei, cells were transfected, processed, and stained using the ProLong Diamond Antifade reagent with DAPI, and imaged by fluorescence microscopy; at least 2×10^3 (for HTC/C3) and 3×10^3 (for 8505C) cells were counted for each sample, and the number of cells with abnormal nuclei was expressed as percentage of the total count. For evaluation of γH2AX-positive cells, at least 650 cells for each sample were counted and the number of γH2AX-positive cells was expressed as percentage of the total count.

2.8. Western blot analysis

Protein extraction and western blot analysis were performed as previously described [31]. The following antibodies were used: anti-MASTL (ab86387, 1:7000) from Abcam, Cambridge, UK; anti-cleaved-PARP (Asp241, #9541, 1:1000) and anti-cleaved Caspase 3 (Asp175, #9664, 1:1000) from Cell Signaling Technology, Danvers, MA, USA; γH2AX (A300-081A-M, 1:1000) from Bethyl Laboratories, Montgomery, TX, USA; anti-Actin (A2066, 1:5000); anti-β-Tubulin (clone TUB 2.1, T4026, 1:4000) from Sigma-Aldrich, St Louis, MO, USA; anti-GAPDH (sc-3223, 1:1000) from Santa Cruz, CA, USA.

2.9. Time-lapse video microscopy

Time-lapse phase-contrast video microscopy was carried out on cells seeded in 24-well plates, transfected with 20 nM MASTL and NT siRNA oligos, and cultured in a Cell-IQ SLF instrument (CM Technology Oy, Tampere, Finland). Phase-contrast images were taken every 30 min for at least 4 days after siRNA transfection by a 10X inverted objective. Videos were prepared using the Export video tool of the Cell-IQ Analyser software. Size of GFP-positive nuclei was analyzed by employing the Cell-IQ Analyser Pro-Write software.

2.10. Annexin V apoptosis assay

Cells (1.9×10^5) were seeded in 60 mm dishes and transfected with siRNAs. Both adherent and floating cells were collected 48, 72, 96, and 120 h after transfection and processed with FITC Annexin V Apoptosis Detection Kit (Becton Dickinson, San Jose, CA, USA), according to the manufacturer's instructions; TO-PRO-3 iodide (1:2000; Invitrogen/Molecular Probes®) was used for DNA staining. Samples were acquired using BD FACSCanto instrument (Becton Dickinson, San Jose, CA, USA) and analyzed with FlowJo v7.6 software (TreeStar).

3. Results

3.1. MASTL expression in thyroid tumors

We have previously identified MASTL as an example of "non-oncogene addiction" in thyroid cancer. Indeed, siRNA-based functional screening identified MASTL among a list of genes whose inhibition affected the growth of thyroid tumor cell lines, while sparing that of immortalized normal thyrocytes. Moreover, the MASTL gene is not mutated in thyroid tumors, and is not overexpressed in thyroid tumor samples and cell lines [18]. Herein, we investigated the expression of MASTL protein in a proprietary thyroid tumor collection by immunohistochemical analysis. Thirty-nine archival paraffin-embedded sections, 28 of which including both tumor and normal tissue were analyzed. A semiquantitative assessment of the MASTL immunostaining (H-score) was undertaken considering both the intensity and extent of cell staining [29]. As shown in Fig. 1A (left), the median MASTL protein expression was similar between tumor and normal thyroid tissues. The lack of substantial differences was highlighted when only tumor and matched normal samples were compared (Fig. 1A, right). Fig. 1B documents the comparable expression of MASTL in thyroid tumor and surrounding normal tissues in four representative samples.

3.2. MASTL knockdown hinders proliferation of thyroid tumor cells

The previously reported dependency of thyroid tumor cells on MASTL activity [18] was further investigated by assessing the effects of MASTL silencing on the growth of two ATC-derived cell lines, namely HTC/C3 and 8505C. Cells were transfected with control (siNT) and three MASTL (siMASTL #1, #4, and #5) siRNAs; the following day, cells were split into plates and then employed for proliferation assay or western blot analysis. For both cell lines, CellTiter-Glo assay revealed growth reduction of cells transfected with the three siMASTL in comparison to siNT transfected cells (Fig. 2A, top). Indeed, for HTC/C3, the increase in cell number at day 6, vs. that day 1, was 7 fold for control and 5–6 fold for MASTL-depleted cells. The same was observed for 8505C: at day 7, vs. day 1, the increase in cell number was 9 fold for control, whereas it was 7–8 fold for MASTL-depleted cells. The reduction in MASTL protein expression was documented by western blot at 48 h after siRNA transfection (Fig. 2A, middle). Of note, we microscopically observed that, at variance with control, MASTL-depleted HTC/C3 and 8505C cells exhibited altered morphology, such as giant cells with multiple nuclei (Fig. 2A, bottom) and an increase in floating cells at later time points (data not shown). The growth inhibitory effect of MASTL was further corroborated by the crystal violet assay performed at 7 days after transfection (Fig. 2B): depletion of MASTL, with all three siRNAs, reduced the growth of both cell lines in comparison with control. In particular, the three MASTL siRNA #1, #4, and #5 reduced, respectively, the growth of HTC/C3 cells by 27.2%, 18.4% and 72.9%, and that of 8505C cells by 35.3%, 20.2%, and 68.9%.

Overall, these results demonstrate that thyroid tumor cell proliferation requires MASTL activity.

3.3. MASTL-depleted cells exhibit abnormal nuclei and aberrant mitotic figures

As anticipated in the previous paragraph, at variance with siNT control, MASTL-depleted HTC/C3 and 8505C cells exhibited altered

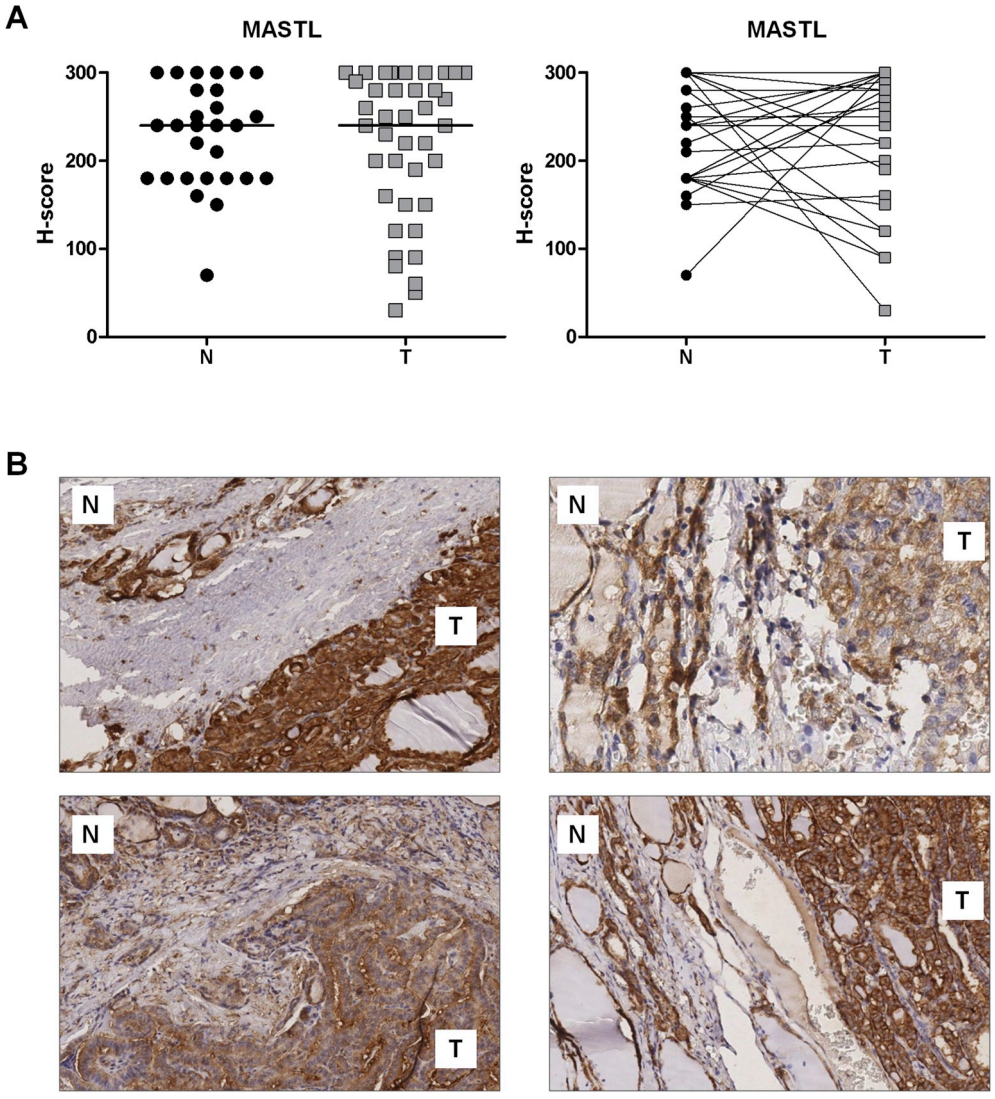

Fig. 1. Detection of MASTL expression in thyroid cancer tissues by immunohistochemistry. (A) ***Left:*** scatter dot plot distribution of H-score values measuring MASTL expression in a proprietary collection of 39 thyroid tumor (T) and 28 normal (N) samples; in the graph the median is recorded. ***Right:*** paired dot plot of H-score values of 28 matched thyroid tumor and normal samples. **(B)** Examples of the immunohistochemical results in four representative cases, showing a consistent MASTL immunoreactivity between tumor (T) and normal cells (N) (40X magnification).

morphology, such as giant cells with multiple nuclei (Fig. 2A, bottom). Multinucleated giant cells displayed abnormal nuclei, such as multiple/lobate nuclei, nuclear blebs, and micronuclei [32], which can originate from errors in mitosis, including those caused by MASTL depletion [4]. Of note, we have previously reported non-quantitative evidence of nuclear abnormalities in 8505C MASTL-depleted cells [18]. To further investigate the previously listed nuclear aberrations in our experimental setting, HTC/C3 and 8505C cells transfected with control and MASTL siRNAs were stained with DAPI and scored for the presence of aberrant nuclear structures (Fig. 3A). In both cell lines, MASTL depletion significantly increased the percentage of nuclear abnormalities compared to control. The nuclear anomalies were observed for HTC/C3 in 16.9% of siMASTL #1-cells, 19.3% of siMASTL #4-cells, and 21.1% of siMASTL #5-cells, but only in 6.1% of control cells; similarly, nuclear anomalies were observed in 8505C cells, and were present in 28.1% of siMASTL #1-cells, 36.8% of siMASTL #4-cells and 41.1% of siMASTL #5-cells, in comparison to 14% for siNT.

We next investigated the occurrence of mitotic aberrations in MASTL-depleted HTC/C3 and 8505C cells by immunofluorescence analysis for microtubules (β-tubulin), phosphorylated histone H3 on serine 10, and nuclei (DAPI). The results are reported in Fig. 3B: in comparison to normal mitoses in control cells (*a* and *e*), MASTL-depleted cells were characterized by the presence of lagging chromosomes (*b*, *c* and *g*), unbalanced chromosome segregation (*d*), DNA bridges connecting daughter cells (*f*), and multipolar mitosis with lagging chromosomes (*h*). Together, these data suggest that MASTL knockdown perturbs mitotic cell division, thus give rise to cells with abnormal nuclei.

The perturbation of mitosis upon MASTL depletion was also documented by time-lapse phase-contrast and fluorescence microscopy of control and MASTL-depleted HTC/C3 and 8505C cells stably expressing the GFP-tagged histone H2B (H2B-GFP) (hereafter called HTC/C3_H2B-GFP and 8505C_H2B-GFP cells). Different from control cells, which proliferated and displayed normal mitosis, reaching confluence at the end of the experiment, cells silenced for MASTL showed severe defects in mitotic cell division, with consequent growth impairment. The majority of HTC/C3_ H2B-GFP cells transfected with siMASTL#1 and #4 did not undergo mitosis and, as a consequence, formed abnormally nucleated giant cells. Mitotic impairment was even more evident in siMASTL#5 cells which were not able to complete mitosis and eventually died (Supplementary videos). To a lesser extent, MASTL-depleted 8505C_H2B-GFP cells also had the same phenotype (Supplementary

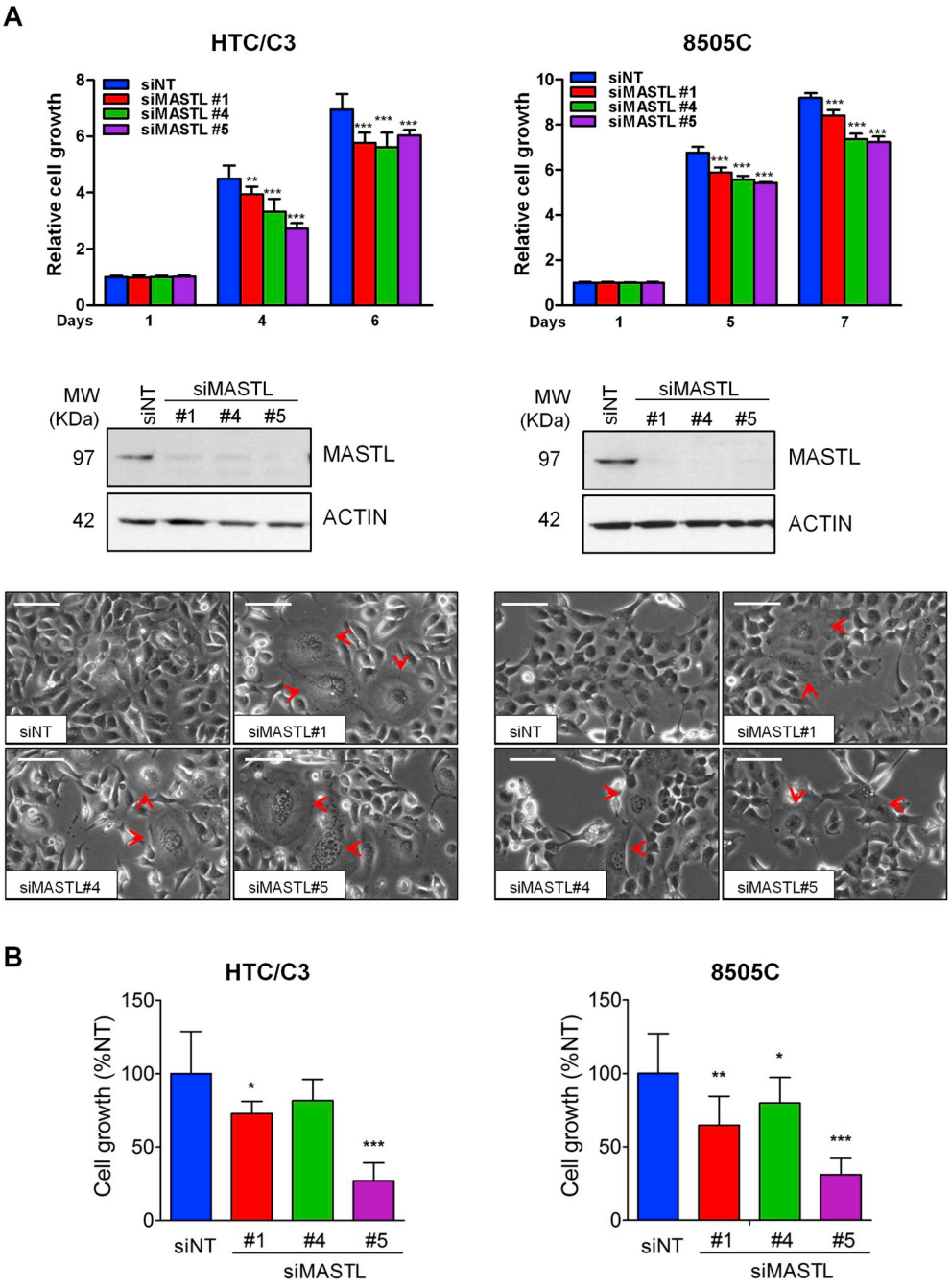

Fig. 2. MASTL knockdown impairs ATC cell growth. **(A)** HTC/C3 and 8505C cells were transfected with control (siNT) and MASTL siRNAs, and split the following day. ***Top:*** Cell growth determined by CellTiter-Glo assay at the indicated time points after splitting; values are plotted as mean ± sd and normalized to values on day 1. ***Middle:*** Western blot analysis of MASTL expression in siRNAs-transfected HTC/C3 and 8505C cells at day 1 after splitting (2 days after transfection); actin represents loading control. ***Bottom:*** representative images of siRNAs transfected HTC/C3 and 8505C cells at 5 and 4 days after transfection, respectively. Giant cells with multiple nuclei are indicated by arrowheads. Scalebar = 100 µm. **(B)** Growth assay of HTC/C3 and 8505C cells 7 days after transfection with the indicated siRNAs; values represent optical density of crystal violet normalized to control values, and are indicated as mean ± sd of two (for HTC/C3) or three (for 8505C) independent experiments. In A (top) and B, an unpaired Student's t-test was used to compare MASTL siRNAs vs control (*p < 0.05; **p < 0.01; ***p < 0.001).

videos). Size analysis of GFP-positive nuclei showed that siMASTL HTC/C3_H2B-GFP cells displayed an increase in cells with double nuclei (ranging from 42.7% to 68.9% for #1, 38.5%–60.9% for #4, and 44.1%–84.1% for #5), compared to siNT (ranging from 30.8% to 47.4%) (Fig. 3C).

Supplementary video related to this article can be found at https://doi.org/10.1016/j.canlet.2018.11.010.

On the whole, MASTL-depleted thyroid tumor cells display aberrant mitosis, abnormal nuclei, and micronuclei, features that are indicative of mitotic catastrophe.

3.4. Depletion of MASTL associates with an increase in γH2AX

It is well established that aberrant mitosis and nuclear abnormalities are often associated with DNA double strand breaks (DSBs) [33]. To investigate this association in MASTL-depleted thyroid tumor cells we performed immunofluorescence analysis on control (siNT) and MASTL-depleted (siMASTL #1, #4 and #5) HTC/C3 and 8505C cells for phosphorylated histone H2AX on serine 129 (referred to as γH2AX), an established marker of DNA DSBs [34]; the analysis was performed at 72 h after siRNA transfection (Fig. 4A). The percentage of γH2AX-positive cells was significantly higher in MASTL-depleted cells than in control in both HTC/C3 and 8505C cells. In addition to cells bearing distinct γH2AX foci, we also detected cells that displayed pan-nuclear γH2AX staining. The percentage of cells carrying γH2AX foci was significantly higher (at least 2 fold) in MASTL-depleted cells with respect to control in both HTC/C3 and 8505C cells, indicating an increase of DNA DSBs. Interestingly, the presence of γH2AX foci was often associated with marked nuclear abnormalities (Fig. 4A, bottom), supporting the notion that DNA DSBs may be produced by aberrant cell division. With respect to cells bearing pan-nuclear γH2AX staining, which is considered to be associated with apoptosis [35], we observed an

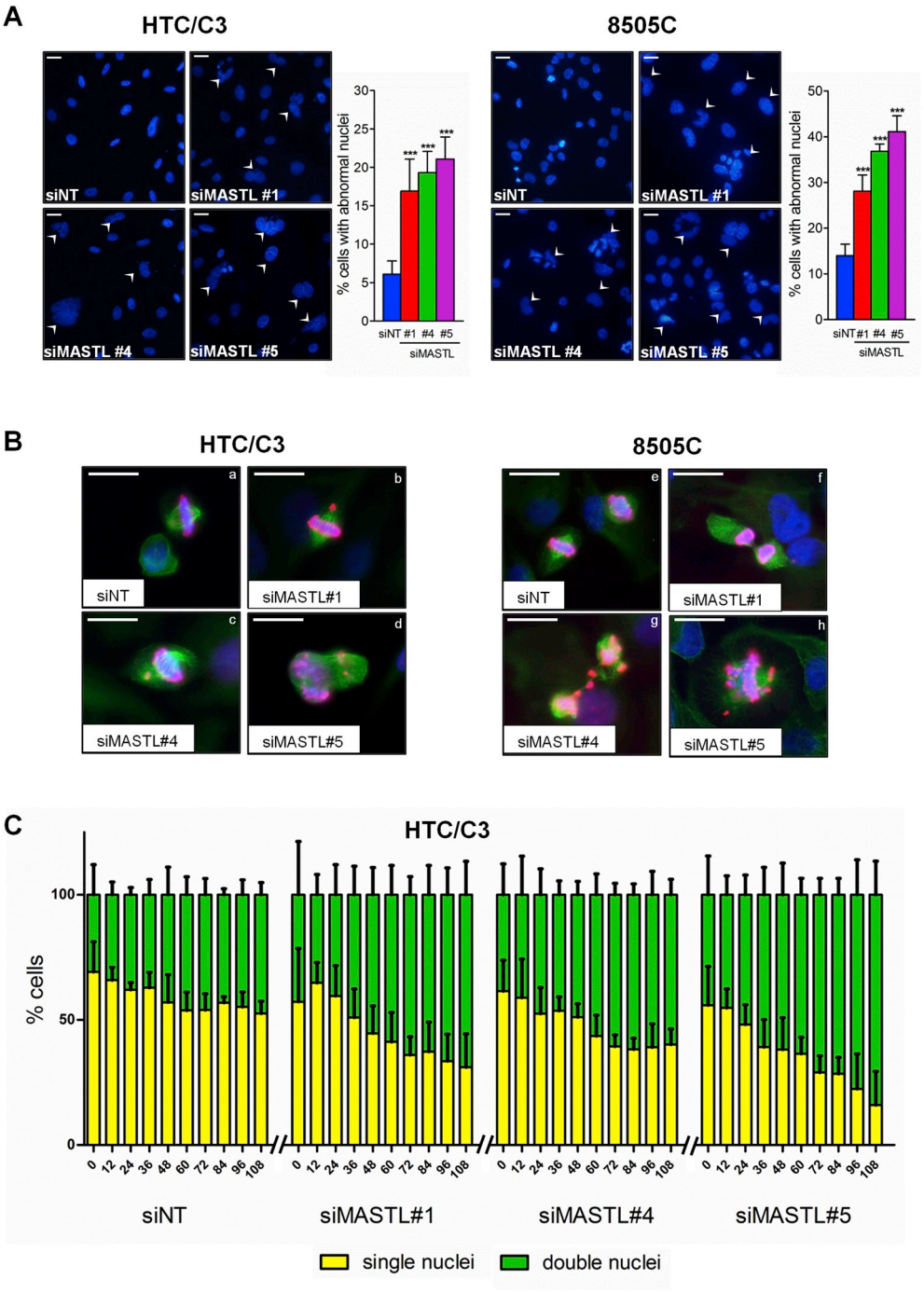

Fig. 3. Depletion of MASTL induces abnormal nuclei and mitotic aberrations. HTC/C3 and 8505C cells were transfected with the indicated siRNAs and analyzed 5 and 4 days later, respectively. **(A)** Representative images of cells stained for nuclei (blue, DAPI); cells with nuclear aberrations are indicated by arrowheads. The graphs represent the corresponding quantification; for each set, the percentage of abnormal nuclei (represented as mean ± sd) was determined by counting a total number of 2×10^3 cells for HTC/C3 and 3×10^3 cells for 8505C from at least 6 independent experiments; an unpaired Student's t-test was used to compare control *vs* MASTL siRNAs; asterisks indicate statistical significance (***$p < 0.001$). **(B)** Representative images of immunofluorescence from cells stained for microtubules (β-tubulin, green), phosphorylated histone H3 (Ser10) (pH3, red) and nuclei (DAPI, blue). Scalebar = 50 μm. **(C)** Time-lapse analysis of HTC/C3 cells at the indicated time points (hours) after transfection with control and MASTL siRNAs. Histograms represent the percentage of HTC/C3 cells displaying single (yellow) and double nuclei (green), plotted as mean ± sd of three independent experiments; size of GFP-positive nuclei was analyzed with CellIQ Analyser Pro-Write software and the number of cells with single or double nuclei was recorded during the entire experiment.

increase in MASTL-depleted HTC/C3, but not in 8505C cells. This finding may be related to the different timing of the cell death process in the two cell lines. Indeed, at the same time point of immunofluorescence analysis (72 h after siRNA transfection), cell death was more evident in HTC/C3 than in 8505C cells (see Fig. 5 and Table S1). We further documented the increase of γH2AX in MASTL-depleted cells by immunoblotting. Together with the efficient MASTL silencing as early as 48 h after siRNA#5 transfection, a gradual increase of γH2AX expression levels in both MASTL-depleted cell lines was observed, starting from 72 h after transfection (Fig. 4B). Similar results were obtained in cells transfected with siRNA #1 and #4 (Supplementary Figure S1).

3.5. MASTL knockdown is associated with thyroid tumor cell death

Mitotic catastrophe characterized by the presence of aberrant mitosis, abnormal nuclei, and micronuclei is an event preceding cell death by apoptotic and non-apoptotic mechanisms [36]. We investigated the occurrence of cell death upon MASTL depletion. HTC/C3 and 8505C cells were transfected with control (siNT) and MASTL (siMASTL #5) siRNAs and analyzed at different time points. The reduction of MASTL protein expression was documented by western blot (Supplementary Figure S2). Starting from 72 h after transfection, we observed the previously described morphological changes and an increase in floating cells in MASTL-depleted HTC/C3 and 8505C cells (data not shown). Annexin V assay followed by flow cytometry analysis showed that

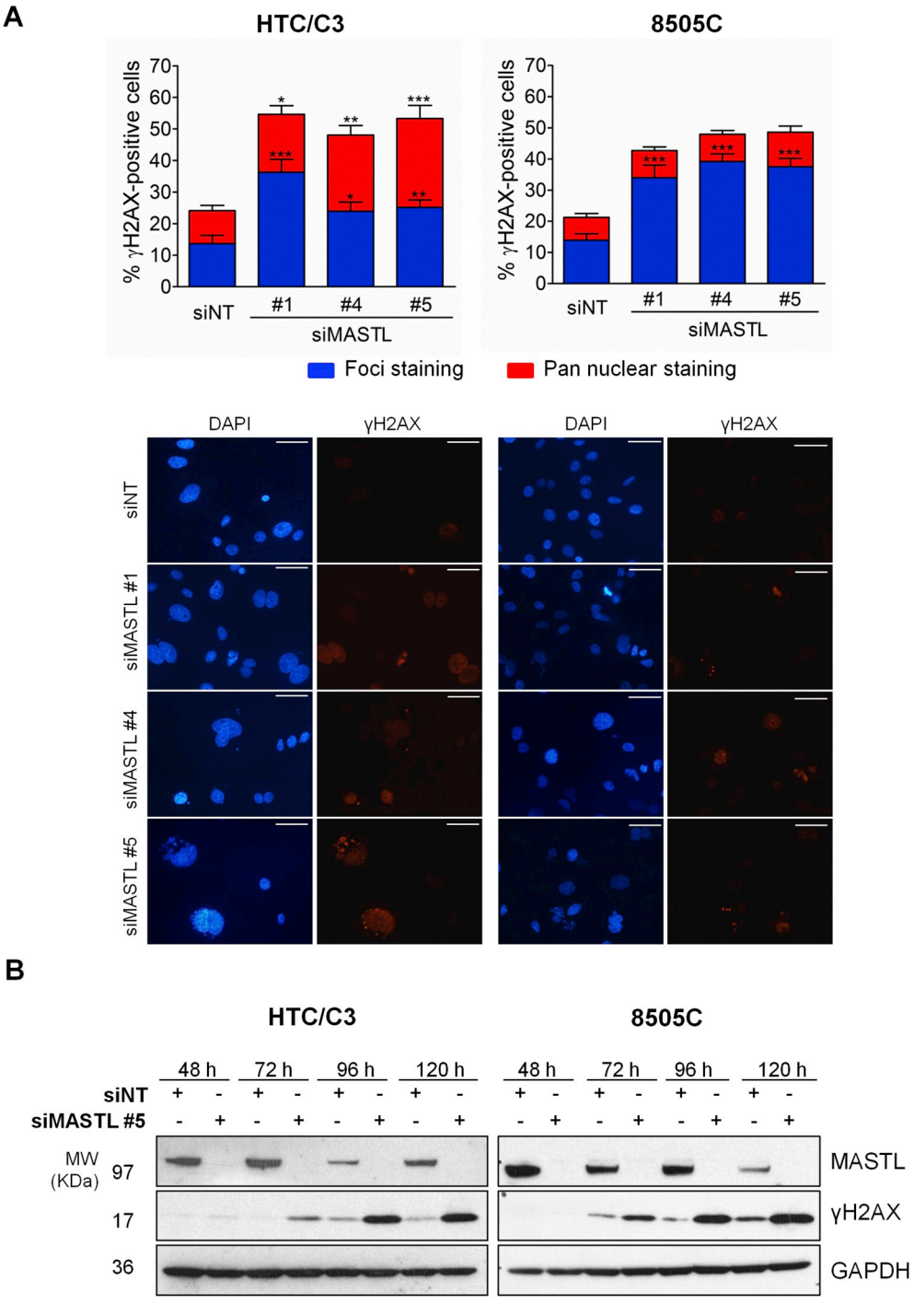

Fig. 4. MASTL silencing increases the amount of γH2AX. (A) HTC/C3 and 8505C cells were transfected with the indicated siRNAs, stained 72 h later for γH2AX (red) and nuclei (DAPI, blue), and imaged by immunofluorescence microscopy. ***Top:*** Percentage of HTC/C3 and 8505C γH2AX-positive cells displaying focal (blue) or diffuse (red) staining; for each sample at least 650 cells were counted; the asterisks indicate significant differences by the unpaired Student's t-test (*$p < 0.05$, **$p < 0.01$, ***$p < 0.001$). ***Bottom:*** representative pictures showing the presence of γH2AX foci in abnormal nuclei. Scalebar = 100 μm. **(B)** Western blot analysis of MASTL and γH2AX expression in HTC/C3 and 8505C cells at the indicated time points after siRNA transfection; GAPDH was used as loading control. A representative analysis of three independent experiments is shown.

MASTL depletion was associated with a gradual decrease in the percentage of viable cells. For HTC/C3 (Fig. 5, top, and Supplementary Table S1), while the percentage of viable (TO-PRO-3 negative) control cells remained relatively constant over time (87.5–78.8%), MASTL-depleted viable cells decreased from 87.9% at 48 h to 43.3% at 120 h after transfection. Concomitantly, from 72 h onwards, we observed a consistent increase of the number of siMASTL-HTC/C3 dead cells (TO-PRO-3 positive), increasing from 12.1% at 48 h to 56.7% at 120 h after transfection, whereas control dead cells were in the range of 12.5–21.1%. Similar results were obtained in 8505C cells (Fig. 5, bottom, and Supplementary Table S1): while viable control cells remained constant (90.2–93.9%), MASTL-depleted viable cells decreased from 86.6% at 48 h to 70.6% at 120 h after transfection. At the same time, the number of MASTL-depleted dead cells increased from 13.4% at 48 h to 29.5% at 120 h after transfection, in comparison to control cells which ranged from 6.1 to 9.8%. The majority of dead cells displayed apoptotic feature (TO-PRO-3 positive/Annexin V positive). The occurrence of apoptotic cell death was confirmed by western blot analysis (Fig. 6). For both cell lines, efficient MASTL silencing detectable as early as 48 h after siRNA transfection was associated with increased expression of the apoptotic markers cleaved caspase 3 and cleaved PARP, starting from 72 h after siRNA transfection. Of note, this finding is consistent with the pan-nuclear γH2AX staining we previously observed by immunofluorescence at the same time point in siMASTL-HTC/C3 cells (Fig. 4).

On the whole, these results demonstrate an association between

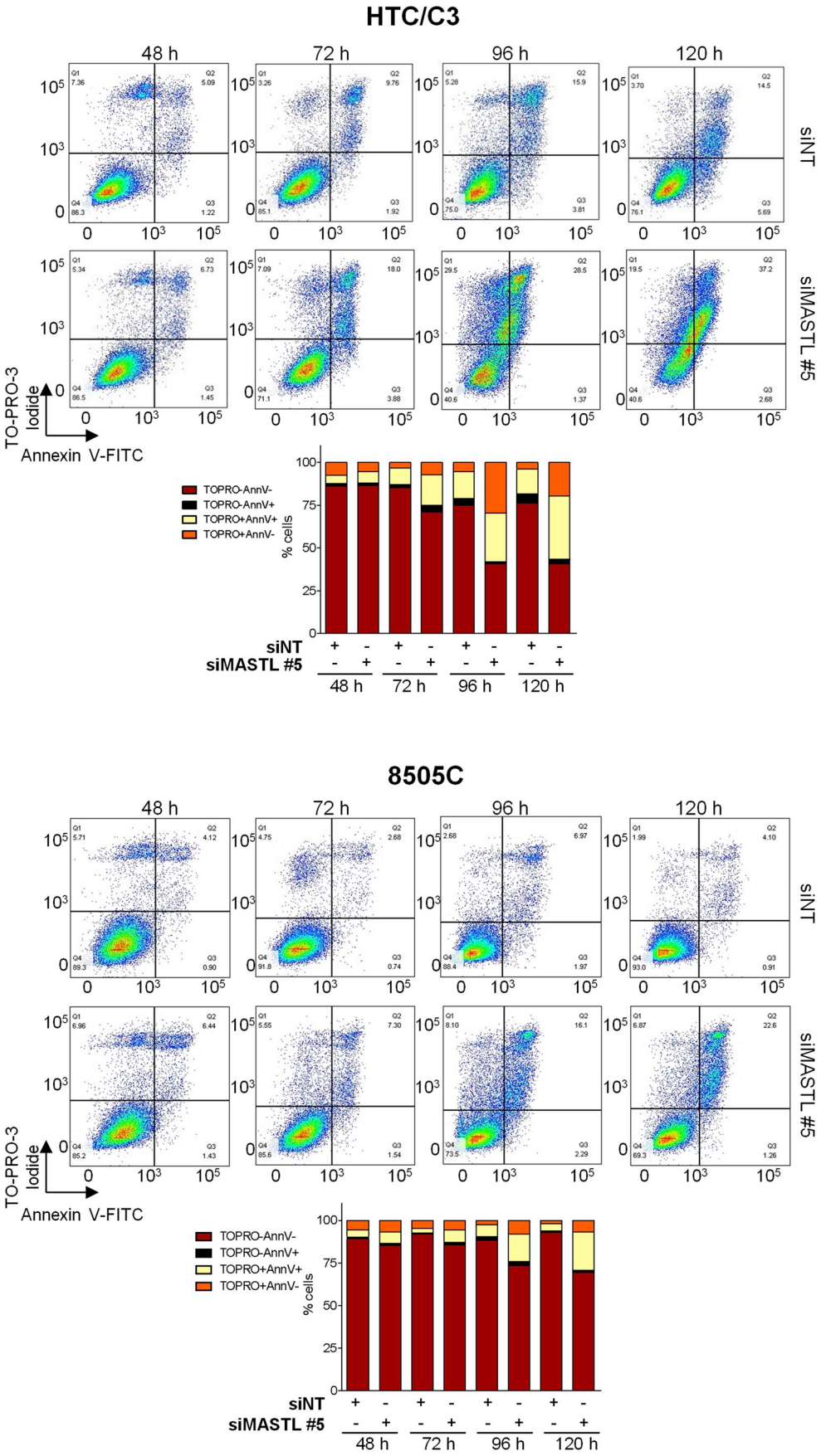

Fig. 5. Knockdown of MASTL is associated with cell death. HTC/C3 and 8505C cells were transfected with control (siNT) or MASTL (siMASTL #5) siRNAs and analyzed at the indicated time points after transfection. Cells were stained with TO-PRO-3 and FITC Annexin V in order to discriminate the percentage of viable and dead cells. For each cell line, representative dot plot (top) and histogram representations (bottom) of FCM analysis are shown; one representative analysis of three (for HTC/C3) and two (for 8505C) independent experiments is shown.

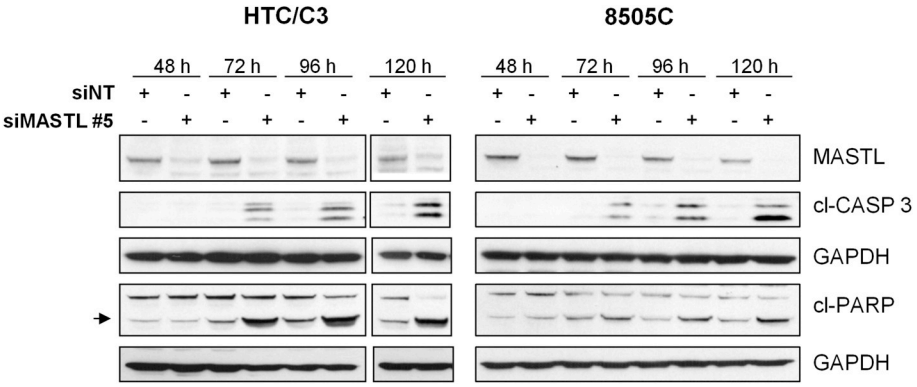

Fig. 6. Detection of apoptotic markers in MASTL-depleted cells. HTC/C3 and 8505C cells were transfected with control (siNT) or MASTL (siMASTL #5) siRNAs and analyzed at the indicated time points after transfection by western blot analysis for the expression of MASTL, cleaved Caspase 3, and cleaved PARP (arrowhead); GAPDH was used as loading control; cleaved PARP expression in the same cell extracts was assessed in a different gel. One representative analysis of three independent experiments is shown for each cell line.

MASTL depletion and the occurrence of thyroid tumor cell death, thus supporting a role of MASTL in regulation of growth and viability of thyroid tumor cells.

3.6. *MASTL knock-down enhances thyroid tumor cell sensitivity to cisplatin*

The DNA damaging drug cisplatin is one of the most commonly used chemotherapeutic agents for treatment of various tumors, including anaplastic and metastatic thyroid cancers [37,38]. Unfortunately, cisplatin is usually ineffective in thyroid tumors due to drug resistance and toxicity, and does not improve overall patient survival [39]. Herein, we investigated whether MASTL depletion, which enhances DNA damage, is able to sensitize thyroid tumor cells to cisplatin, as already described for other tumor types [10,40]. Towards this aim, 8505C and HTC/C3 cells were transfected with siMASTL#5 and two days later were treated for 48 h with increasing doses of cisplatin, whose toxicity in both cell lines has been previously assessed. Cells were then assessed for viability by CellTiter-Glo assay. The dose-response curves reported in Fig. 7A show that while sensitivity to increasing doses of cisplatin was similar in parental and siNT-transfected cells, it consistently increases in MASTL-depleted cells. The reduced cell viability in the presence of cisplatin (10 μM and 20 μM for 8505C cells, 3 μM for HTC/C3) is more evident as shown in Fig. 7B: MASTL depletion led to a appreciable decrease of viability (by 35% in 8505C cells and 55% in HTC/C3 cells in comparison to the siNT control), which was emphasized when cells were treated with cisplatin (by 65–82% in 8505C cells and 83% in HTC/C3 cells).

On the whole, these observations support the premise that MASTL depletion induces chemosensitivity in thyroid tumor cells.

4. Discussion

The mitotic kinase MASTL has recently emerged as promising therapeutic target for cancer treatment. MASTL overexpression has been observed in several solid tumors [9,10], and in breast cancer is associated with poor prognosis [11]. MASTL inhibition is able to reduce the viability of head and neck tumor cells when combined with cisplatin treatment [10] and of non small cell lung cancer cells when combined with radiation therapy [13]. Notably, both these studies reported that MASTL inhibition alone has a partial [10] or null [13] growth inhibitory effect on tumor cells. Furthermore, it was very recently demonstrated that MASTL inhibition reduces the growth of breast cancer cells both *in vitro* and *in vivo* and enhances radiosensitivity [11,15]. No effect of MASTL depletion on normal cells has been observed [10,15].

To date, the role of MASTL in the regulation of thyroid tumor cell biology has been never explored. We identified MASTL as vulnerability for this tumor type. Indeed, a siRNA-based functional screening identified MASTL among a list of genes whose inhibition affected the growth

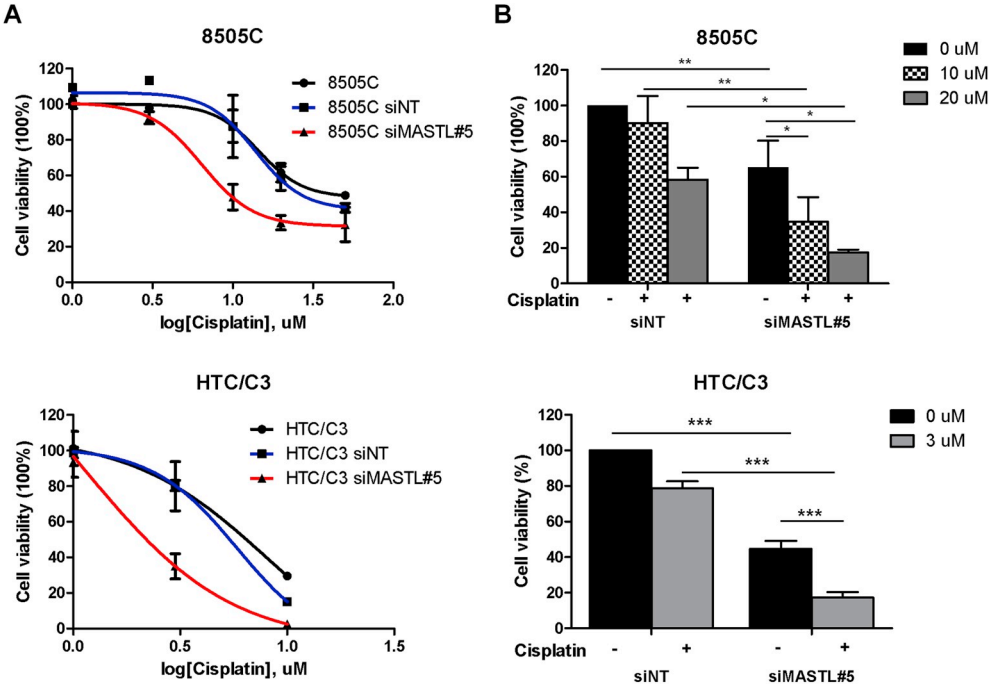

Fig. 7. MASTL depletion sensitized thyroid tumor cells to cisplatin. (A) Dose-response curves of parental and siNT/MASTL#5-transfected cells treated, two days after transfection, with increasing concentration of cisplatin (1, 3, 10, 20, 50 μM for 8505C cells; 1, 3, 10 μM for HTC/C3 cells) up to 48 h. The cell viability was determined by Cell-Titer Glo assay. Data are expressed as mean ± sd of four independent experiments in triplicate. **(B)** Histograms represent cell viability values from A, normalized to siNT control values (100%); the asterisks indicate significant differences by the unpaired Student's t-test (*$p < 0.05$, **$p < 0.01$, ***$p < 0.001$).

of thyroid tumor cell lines, while sparing that of immortalized normal thyrocytes. Herein, we first documented the lack of MASTL protein overexpression in a thyroid tumor collection. Indeed, we found that MASTL protein is expressed at comparable level in tumor and normal thyroid tissues, in line with previous gene expression data [18]. This is in agreement with the "non-oncogene addiction" concept, indicating that, and at variance with other tumor types featuring MASTL overexpression, thyroid tumor cells are 'addicted' to the basal activity of MASTL. We further characterized the effects of MASTL depletion in thyroid tumor cells in two ATC-derived cell lines, and observed a considerable reduction of cell growth upon MASTL depletion by siRNA. Furthermore, MASTL-depleted cells displayed mitotic catastrophe, had increased levels of DNA damage and, ultimately, underwent cell death.

The evidence that MASTL inhibition significantly hampers the growth of thyroid tumor cells stresses its relevance as a possible target for thyroid cancer treatment. We further observed the presence of altered size/morphology and aberrant mitotic figures in MASTL-depleted thyroid tumor cells, which were in accordance with what reported as the consequences of MASTL depletion in both normal and tumor cells of different origin [4,5]. The outcome of such aberrant mitoses is referred to as mitotic catastrophe, and is characterized by the formation of large cells with aberrant nuclear structures, such as multiple nuclei, micronuclei, and lobular nuclei [36]. Mitotic catastrophe is a step preceding cell death, which may occur through apoptotic or necrotic mechanisms, either after or during deregulated mitosis [36]. The occurrence of mitotic catastrophe in our experimental setting was further documented by time-lapse microscopy experiments, unequivocally showing impaired mitotic cell division and multinuclear giant cell formation upon MASTL depletion.

As a consequence of chromosome segregation errors during abnormal mitosis [33], cells displaying mitotic catastrophe accumulate chromosomal breaks that eventually trigger a DNA damage response and cell death [41]. In MASTL-depleted cells, we observed increased expression levels, as well as increased foci number, of the DNA DSBs marker γH2AX. MASTL is involved in both the regulation of DNA damage response [7] and maintenance of genome stability during DNA damage response [8]; the contribution of these mechanisms to the increase in DNA damage in MASTL-depleted cells remains to be investigated. Interestingly, we also documented increased pan-nuclear expression of γH2AX upon MASTL depletion, a feature recognized as suggestive of initial apoptosis [35]. Indeed, upon MASTL depletion, we observed increased cell death, definitely involving an apoptotic mechanism, as suggested by both western blot and annexin V assay.

Recently, several studies highlighted a key role for MASTL in regulating chemoresistance; indeed, MASTL inhibition renders cancer cells more sensitive to chemotherapeutic agents such as cisplatin and 5-fluorouracil [10,14,40]. In agreement with these observations, we showed that MASTL depletion enhances the sensitivity of thyroid tumor cells to cisplatin. Since standard chemotherapies for ATC are relatively ineffective [39], the combination of MASTL depletion with chemotherapy could represent a new therapeutic strategy for thyroid cancer.

MASTL depletion has been demonstrated to affect the growth of several tumor cell types as a consequence of mitotic defects [10,11,13,15]. In our experimental model, mitotic catastrophe consequent to MASTL inhibition caused cell death, in agreement with a previous study on MASTL-depleted breast cancer cells [15]. Alvarez-Fernandes et al. [11] reported that the sensitivity of breast tumor cell lines to MASTL depletion is related to the expression level of the B55 subunit of the PPA2/B55 complex, which is inhibited by MASTL activity. Further studies are needed to assess the role of B55 subunit and to identify the molecular requirements of MASTL vulnerability of thyroid tumor cells.

The stimulation of mitotic catastrophe has emerged as a promising strategy for cancer therapy. Treatment with ionizing radiation [42] or with drugs that hinder proper cell division [43] causes mitotic catastrophe features in tumor cells, leading to cell death [44]. With regards to thyroid tumors, the targeting of mitotic regulators has already been explored in preclinical studies: targeting of PLK1 [45] and Aurora kinases [46] through small-molecule inhibitors significantly reduced the growth and induced cell death in ATC-derived cell lines. Our study identifies a novel mitotic target and strengthens the evidence that mitotic regulators are promising targets for thyroid tumor treatment, either alone or in combination with chemotherapy.

On the whole, our study clearly demonstrated that MASTL represents vulnerability for thyroid tumor cells: its inhibition hinders thyroid tumor cell growth and is associated with increased DNA damage, mitotic catastrophe, and cell death, and enhances the sensitivity to cisplatin. The efficacy of MASTL inhibition in preclinical *in vivo* models of thyroid tumors remains to be investigated. We preliminarily attempted this issue by local treatment of 8505C mouse tumor xenografts with siMASTL, but no effects on MASTL gene and protein expression were detected, suggesting that the reagents and experimental conditions must be established for assessing the *in vivo* effects of MASTL depletion. An alternative approach could be the use of small molecule MASTL inhibitors, whose identification is currently underway, and which has been prompted by the increasing evidence of MASTL as a potential target for cancer therapy. Based on determination of the structure of the minimal MASTL kinase domain, Ocasio et al. [16] designed GCK-1, a 'first generation inhibitor' that can inhibit MASTL kinase activity and cause cellular phenotypes similar to those observed upon MASTL siRNA treatment. Very recently, through virtual screening of natural and synthetic compounds, Ammarah et al. [17] identified a list of putative MASTL inhibitors, among which the synthetic compound ZINC53845290 exhibited promising binding activity. The availability of MASTL inhibitors holds great promise for studies aimed at assessing the efficacy of MASTL inhibition in preclinical models, and to further validate MASTL as a therapeutic target for thyroid and other tumor types.

Author disclosure statement

The authors have nothing to disclose.

Acknowledgments

We thank Dr. Silvana Pilotti (Department of Pathology, Fondazione IRCCS Istituto Nazionale dei Tumori, Milan, Italy) for thyroid sample selection and revision, Mrs. Gabriella Abolafio (Flow Cytometry Facility of Fondazione IRCCS Istituto Nazionale dei Tumori, Milan, Italy) for technical help and Mrs Silvia Grassi for secretarial assistance. The authors also acknowledge Dr. Patrick Moore for manuscript editing. This work was supported by Associazione Italiana per la Ricerca sul Cancro [Grant IG 18395, 2017 to A. Greco].

Appendix A. Supplementary data

Supplementary data to this article can be found online at https://doi.org/10.1016/j.canlet.2018.11.010.

References

[1] C. Dominguez-Brauer, K.L. Thu, J.M. Mason, H. Blaser, M.R. Bray, T.W. Mak, Targeting mitosis in cancer: emerging strategies, Mol. Cell. 60 (2015) 524–536.
[2] E. Mukhtar, V.M. Adhami, H. Mukhtar, Targeting microtubules by natural agents for cancer therapy, Mol. Canc. Therapeut. 13 (2014) 275–284.
[3] T. Otto, P. Sicinski, Cell cycle proteins as promising targets in cancer therapy, Nat.Rev.Cancer. 17 (2017) 93–115.
[4] A. Burgess, S. Vigneron, E. Brioudes, J.C. Labbe, T. Lorca, A. Castro, Loss of human Greatwall results in G2 arrest and multiple mitotic defects due to deregulation of the cyclin B-Cdc2/PP2A balance, Proc. Natl. Acad. Sci. U. S. A 107 (2010) 12564–12569.
[5] M. Alvarez-Fernandez, R. Sanchez-Martinez, B. Sanz-Castillo, P.P. Gan, M. Sanz-Flores, M. Trakala, M. Ruiz-Torres, T. Lorca, A. Castro, M. Malumbres, Greatwall is essential to prevent mitotic collapse after nuclear envelope breakdown in mammals, Proc. Natl. Acad. Sci. U. S. A 110 (2013) 17374–17379.

[6] C. Wurzenberger, D.W. Gerlich, Phosphatases: providing safe passage through mitotic exit, Nat. Rev. Mol. Cell Biol. 12 (2011) 469–482.
[7] A. Peng, T.M. Yamamoto, M.L. Goldberg, J.L. Maller, A novel role for greatwall kinase in recovery from DNA damage, Cell Cycle 9 (2010) 4364–4369.
[8] P.Y. Wong, H.T. Ma, H.J. Lee, R.Y. Poon, MASTL(Greatwall) regulates DNA damage responses by coordinating mitotic entry after checkpoint recovery and APC/C activation, Sci. Rep. 6 (2016) 22230.
[9] J. Vera, L. Lartigue, S. Vigneron, G. Gadea, V. Gire, M. Del Rio, I. Soubeyran, F. Chibon, T. Lorca, A. Castro, Greatwall promotes cell transformation by hyperactivating AKT in human malignancies, Elife 4 (2015) e10115.
[10] L. Wang, V.Q. Luong, P.J. Giannini, A. Peng, Mastl kinase, a promising therapeutic target, promotes cancer recurrence, Oncotarget 5 (2014) 11479–11489.
[11] M. Alvarez-Fernandez, M. Sanz-Flores, B. Sanz-Castillo, M. Salazar-Roa, D. Partida, E. Zapatero-Solana, H.R. Ali, E. Manchado, S. Lowe, T. VanArsdale, D. Shields, C. Caldas, M. Quintela-Fandino, M. Malumbres, Therapeutic relevance of the PP2A-B55 inhibitory kinase MASTL/Greatwall in breast cancer, Cell Death Differ. 25 (2018) 828–840.
[12] S. Rogers, R.A. McCloy, B.L. Parker, D. Gallego-Ortega, A.M.K. Law, V.T. Chin, J.R.W. Conway, D. Fey, E.K.A. Millar, S. O'Toole, N. Deng, A. Swarbrick, P.D. Chastain, A.J. Cesare, P. Timpson, C.E. Caldon, D.R. Croucher, D.E. James, D.N. Watkins, A. Burgess, MASTL overexpression promotes chromosome instability and metastasis in breast cancer, Oncogene 37 (2018) 4518–4533.
[13] R. Nagel, M. Stigter-van Walsum, M. Buijze, J. van den Berg, I.H. van der Meulen, J. Hodzic, S.R. Piersma, T.V. Pham, C.R. Jimenez, V.W. van Beusechem, R.H. Brakenhoff, Genome-wide siRNA screen identifies the radiosensitizing effect of downregulation of MASTL and FOXM1 in NSCLC, Mol.Cancer Ther. 14 (2015) 1434–1444.
[14] S.B. Uppada, S. Gowrikumar, R. Ahmad, B. Kumar, B. Szeglin, X. Chen, J.J. Smith, S.K. Batra, A.B. Singh, P. Dhawan, MASTL induces Colon Cancer progression and Chemoresistance by promoting Wnt/beta-catenin signaling, Mol. Canc. 17 (2018) 111.
[15] Y.N. Yoon, M.H. Choe, K.Y. Jung, S.G. Hwang, J.S. Oh, J.S. Kim, MASTL inhibition promotes mitotic catastrophe through PP2A activation to inhibit cancer growth and radioresistance in breast cancer cells, BMC Canc. 18 (2018) 716.
[16] C.A. Ocasio, M.B. Rajasekaran, S. Walker, G.D. Le, J. Spencer, F.M. Pearl, S.E. Ward, V. Savic, L.H. Pearl, H. Hochegger, A.W. Oliver, A first generation inhibitor of human Greatwall kinase, enabled by structural and functional characterisation of a minimal kinase domain construct, Oncotarget 7 (2016) 71182–71197.
[17] U. Ammarah, A. Kumar, R. Pal, N.C. Bal, G. Misra, Identification of new inhibitors against human Great wall kinase using in silico approaches, Sci. Rep. 8 (2018) 4894.
[18] M.C. Anania, F. Gasparri, E. Cetti, I. Fraietta, K. Todoerti, C. Miranda, M. Mazzoni, C. Re, R. Colombo, G. Ukmar, S. Camisasca, S. Pagliardini, M. Pierotti, A. Neri, A. Galvani, A. Greco, Identification of thyroid tumor cell vulnerabilities through a siRNA-based functional screening, Oncotarget 6 (2015) 34629–34648.
[19] M.E. Cabanillas, D.G. McFadden, C. Durante, Thyroid cancer, Lancet 388 (2016) 2783–2795.
[20] C. La Vecchia, M. Malvezzi, C. Bosetti, W. Garavello, P. Bertuccio, F. Levi, E. Negri, Thyroid cancer mortality and incidence: a global overview, Int. J. Canc. 136 (2015) 2187–2195.
[21] M.P. Stokkel, C.S. Duchateau, C. Dragoiescu, The value of FDG-PET in the follow-up of differentiated thyroid cancer: a review of the literature, Q. J. Nucl. Med. Mol. Imaging 50 (2006) 78–87.
[22] X.M. Keutgen, S.M. Sadowski, E. Kebebew, Management of anaplastic thyroid cancer, Gland Surg. 4 (2015) 44–51.
[23] M.E. Cabanillas, M. Zafereo, G.B. Gunn, R. Ferrarotto, Anaplastic thyroid carcinoma: treatment in the age of molecular targeted therapy, J Oncol Pract 12 (2016) 511–518.
[24] J. Luo, N.L. Solimini, S.J. Elledge, Principles of cancer therapy: oncogene and non-oncogene addiction, Cell 136 (2009) 823–837.
[25] R. Nagel, E.A. Semenova, A. Berns, Drugging the addict: non-oncogene addiction as a target for cancer therapy, EMBO Rep. 17 (2016) 1516–1531.
[26] S.E. Mohr, J.A. Smith, C.E. Shamu, R.A. Neumuller, N. Perrimon, RNAi screening comes of age: improved techniques and complementary approaches, Nat. Rev. Mol. Cell Biol. 15 (2014) 591–600.
[27] M.C. Anania, E. Cetti, D. Lecis, K. Todoerti, A. Gulino, G. Mauro, T. Di Marco, L. Cleris, S. Pagliardini, G. Manenti, B. Belmonte, C. Tripodo, A. Neri, A. Greco, Targeting COPZ1 non-oncogene addiction counteracts the viability of thyroid tumor cells, Cancer Lett. 410 (2017) 201–211.
[28] R.A. Delellis, R.V. Lloyd, P.U. Heitz, C. Eng, Pathology and genetics of tumors of endocrine organs, in: IARC Press (Ed.), World Health Organization Classification of Tumours, IARC Press, Lyon, 20042004.
[29] F.R. Hirsch, M. Varella-Garcia, P.A. Bunn Jr., M.V. Di Maria, R. Veve, R.M. Bremmes, A.E. Baron, C. Zeng, W.A. Franklin, Epidermal growth factor receptor in non-small-cell lung carcinomas: correlation between gene copy number and protein expression and impact on prognosis, J. Clin. Oncol. 21 (2003) 3798–3807.
[30] T. Kanda, K.F. Sullivan, G.M. Wahl, Histone-GFP fusion protein enables sensitive analysis of chromosome dynamics in living mammalian cells, Curr. Biol. 8 (1998) 377–385.
[31] M.G. Vizioli, M. Sensi, C. Miranda, L. Cleris, F. Formelli, M.C. Anania, M.A. Pierotti, A. Greco, IGFBP7: an oncosuppressor gene in thyroid carcinogenesis, Oncogene 29 (2010) 3835–3844.
[32] M. Fenech, M. Kirsch-Volders, A.T. Natarajan, J. Surralles, J.W. Crott, J. Parry, H. Norppa, D.A. Eastmond, J.D. Tucker, P. Thomas, Molecular mechanisms of micronucleus, nucleoplasmic bridge and nuclear bud formation in mammalian and human cells, Mutagenesis 26 (2011) 125–132.
[33] A. Janssen, B.M. van der, K. Szuhai, G.J. Kops, R.H. Medema, Chromosome segregation errors as a cause of DNA damage and structural chromosome aberrations, Science 333 (2011) 1895–1898.
[34] E.P. Rogakou, C. Boon, C. Redon, W.M. Bonner, Megabase chromatin domains involved in DNA double-strand breaks in vivo, J. Cell Biol. 146 (1999) 905–916.
[35] D. Ding, Y. Zhang, J. Wang, X. Zhang, Y. Gao, l. Yin, Q. Li, J. Li, H. Chen, Induction and inhibition of the pan-nuclear gamma-H2AX response in resting human peripheral blood lymphocytes after X-ray irradiation, Cell Death Dis. 2 (16011) (2016).
[36] H. Vakifahmetoglu, M. Olsson, B. Zhivotovsky, Death through a tragedy: mitotic catastrophe, Cell Death Differ. 15 (2008) 1153–1162.
[37] O. Derbel, S. Limem, C. Segura-Ferlay, J.C. Lifante, C. Carrie, J.L. Peix, F. Borson-Chazot, C. Bournaud, J.P. Droz, F.C. de la, Results of combined treatment of anaplastic thyroid carcinoma (ATC), BMC Canc. 11 (2011) 469.
[38] A. Seto, I. Sugitani, K. Toda, K. Kawabata, S. Takahashi, T. Saotome, Chemotherapy for anaplastic thyroid cancer using docetaxel and cisplatin: report of eight cases, Surg. Today 45 (2015) 221–226.
[39] R.C. Smallridge, L.A. Marlow, J.A. Copland, Anaplastic thyroid cancer: molecular pathogenesis and emerging therapies, Endocr.Relat Cancer. 16 (2009) 17–44.
[40] J. Tian, Y. Lin, J. Yu, E2F8 confers cisplatin resistance to ER + breast cancer cells via transcriptionally activating MASTL, Biomed. Pharmacother. 92 (2017) 919–926.
[41] G. Imreh, H.V. Norberg, S. Imreh, B. Zhivotovsky, Chromosomal breaks during mitotic catastrophe trigger gammaH2AX-ATM-p53-mediated apoptosis, J. Cell Sci. 124 (2011) 2951–2963.
[42] P. Maier, L. Hartmann, F. Wenz, C. Herskind, Cellular pathways in response to ionizing radiation and their targetability for tumor radiosensitization, Int. J. Mol. Sci. 17 (E102) (2016).
[43] M.M. Mc Gee, Targeting the mitotic catastrophe signaling pathway in cancer, Mediat. Inflamm. 2015 (2015) 146282.
[44] T.V. Denisenko, I.V. Sorokina, V. Gogvadze, B. Zhivotovsky, Mitotic catastrophe and cancer drug resistance: a link that must to be broken, Drug Resist. Updates 24 (2016) 1–12.
[45] M.A. Russo, K.S. Kang, A. Di Cristofano, The PLK1 inhibitor GSK461364A is effective in poorly differentiated and anaplastic thyroid carcinoma cells, independent of the nature of their driver mutations, Thyroid 23 (2013) 1284–1293.
[46] E. Baldini, C. Tuccilli, N. Prinzi, S. Sorrenti, A. Antonelli, L. Gnessi, S. Morrone, C. Moretti, M. Bononi, Y. rlot-Bonnemains, M. D'Armiento, S. Ulisse, Effects of selective inhibitors of Aurora kinases on anaplastic thyroid carcinoma cell lines, Endocr.Relat.Cancer 21 (2014) 797–811.